

PAPER

Doping β -Ga₂O₃ with europium: influence of the implantation and annealing temperature

To cite this article: M Peres *et al* 2017 *J. Phys. D: Appl. Phys.* **50** 325101

View the [article online](#) for updates and enhancements.

Related content

- [Structural and optical characterization of Eu-implanted GaN](#)
K Lorenz, N P Barradas, E Alves *et al.*
- [Enhanced dynamic annealing and optical activation of Eu implanted a-plane GaN](#)
N. Catarino, E. Nogales, N. Franco *et al.*
- [Effect of AlN content on the lattice site location of terbium ions in Al_xGa_{1-x}N compounds](#)
M Fialho, J Rodrigues, S Magalhães *et al.*

Recent citations

- [Review of Ga₂O₃-based optoelectronic devices](#)
D. Guo *et al*
- [Self-Limiting Galvanic Growth of MnO₂ Monolayers on a Liquid Metal—Applied to Photocatalysis](#)
Mohammad B. Ghasemian *et al*
- [pH controlled synthesis of UV excited host-sensitized luminescence in Dy³⁺-doped Ga₂O₃](#)
Guangran Zhang *et al*



IOP | ebooks™

Bringing together innovative digital publishing with leading authors from the global scientific community.

Start exploring the collection—download the first chapter of every title for free.

Doping β -Ga₂O₃ with europium: influence of the implantation and annealing temperature

M Peres¹, K Lorenz¹, E Alves¹, E Nogales², B Méndez², X Biquard³, B Daudin⁴, E G Villora⁵ and K Shimamura⁵

¹ IPFN, Instituto Superior Técnico (IST), Campus Tecnológico e Nuclear, Estrada Nacional 10, P-2695-066 Bobadela LRS, Portugal

² Dpto. Física de Materiales, Universidad Complutense de Madrid, 28040 Madrid, Spain

³ Univ. Grenoble Alpes, CEA, INAC, MEM, F-38000 Grenoble, France

⁴ Univ. Grenoble Alpes, CEA, INAC, PHELIQS, F-38000 Grenoble, France

⁵ National Institute for Materials Science, 1-1 Namiki, Tsukuba 305-0044, Japan

E-mail: marcoperes@ctn.tecnico.ulisboa.pt

Received 16 March 2017, revised 6 June 2017

Accepted for publication 15 June 2017

Published 18 July 2017



Abstract

β -Ga₂O₃ bulk single crystals were doped by ion implantation at temperatures from room temperature to 1000 °C, using a 300 keV Europium beam with a fluence of 1×10^{15} at cm^{-2} . Raising the implantation temperature from room temperature to 400–600 °C resulted in a significant increase of the substitutional Eu fraction and of the number of Eu ions in the 3+ charge state as well as in a considerable decrease of implantation damage. Eu is found in both charge states 2+ and 3+ and their relative fractions are critically dependent on the implantation and annealing temperature, suggesting that defects play an important role in stabilizing one of the charge states. The damage recovery during post-implant annealing is a complex process and typically defect levels first increase for intermediate annealing temperatures and a significant recovery of the crystal only starts around 1000 °C. Cathodoluminescence spectra are dominated by the sharp Eu³⁺ related intra-ionic 4f transition lines in the red spectral region. They show a strong increase of the emission intensity with increasing annealing temperature, in particular for samples implanted at elevated temperature, indicating the optical activation of Eu³⁺ ions. However, no direct correlation of emission intensity and Eu³⁺ fraction was found, again pointing to the important role of defects on the physical properties of these luminescent materials.

Keywords: β -Ga₂O₃, ion implantation, europium, RBS, XANES, cathodoluminescence

(Some figures may appear in colour only in the online journal)

1. Introduction

β -Ga₂O₃ is an emerging semiconductor with a wide band gap of about ~4.9 eV, considerably larger than that of other transparent conducting oxides [1–4]. Recent works have demonstrated a significant potential of this semiconductor for optoelectronic and electronic applications, mainly for high power devices, light emitting diodes (LED), lasers, transparent ‘intelligent’ windows, solar cells, transparent thin-film electroluminescent devices, etc [1, 5–7]. β -Ga₂O₃ is also a promising substrate for high-current vertically structured GaN-LEDs combining the transparency of sapphire with

the conductivity of SiC, the typical substrates for commercial GaN-devices [1, 8–10]. Furthermore, several works have been published establishing β -Ga₂O₃ as a host for rare earth (RE) ions due to its large band gap; most of these studies were based on thin-films and more recently nanostructures [11–15]. It is well known that RE ions have very interesting properties for optoelectronic applications [16–18]. The particular characteristics of RE in the 3+ charge state are their sharp and intense emissions due to the internal transitions in the partially filled 4f electron shell. These transitions are almost insensitive to the local environment thanks to the screening effect of the outer 5s and 5d electrons. It is also well known that the

optical activation of RE ions depends critically on their lattice site location and is affected by the presence of defects, which could be involved in energy transfer processes, act as competitive non-radiative recombination channels or change the RE charge state. Therefore, to improve the optical activation, it is crucial to better understand how the defects participate in the optical processes and affect the coordination environment.

Doping β -Ga₂O₃ with RE during growth is challenging due to low solubility limits in the beta phase and often leads to a second phase segregation [11, 19]. Some recent studies have shown the advantages of ion implantation to dope β -Ga₂O₃ with different RE ions and to overcome the low solubility of these ions [12, 13]. High quality β -Ga₂O₃ bulk single crystals only became available recently [20]. Our preliminary study on Eu implantation into β -Ga₂O₃ bulk crystals with (100) surface orientation has shown that implantation at room temperature (RT) creates a high density of defects which affect the local environment of the implanted ions [12]. For high fluences of 1×10^{15} at cm⁻² and above, Rutherford backscattering spectrometry/channeling (RBS/C) showed the break-down of ion channeling effect close to the surface, usually a sign of amorphisation. In contrast, a recent comprehensive study of implantation damage build-up in (010) β -Ga₂O₃ suggested that no amorphisation occurs [21]. Instead damage saturates at high defect levels possibly due to the formation of a different phase [21, 22]. The effect of the surface orientation itself on these distinct behaviors is still unclear.

Most of these defects induced by ion implantation can be removed by annealing above 1000 °C. However, even after the almost complete recovery of the damage created during the implantation, it was observed that the Eu is still located mostly in random sites and starts to diffuse towards the surface [12]. Nevertheless, optical activation of Eu was achieved in these samples leading to the typical red Eu³⁺ related emission lines [12].

One of the main requisites to get the characteristic, intense and sharp emission of the Eu intra-ionic transitions is to control the fraction of Eu in Ga sites, for which Eu is expected to have a valence state 3+ to keep the charge neutrality. In GaN it was already observed that implantation at higher temperatures reduces the density of the defects created during the implantation, and increases the fraction of substitutional Eu [23, 24]. This effect has been attributed to the increase of the defect mobility with the implantation temperature and hence their ability to recombine during the implantation. In this paper, we study the effect of elevated implantation temperatures on Eu incorporation, defect formation and Eu optical activation in β -Ga₂O₃. Furthermore, the influence of the annealing temperature on the damage profiles, the substitutional fraction, as well as on the charge state will be discussed and correlated with the optical properties of the RE implanted samples.

2. Experimental details

β -Ga₂O₃ single crystals were grown by the floating zone technique. Growth details were previously described in [25]. These crystals were cleaved along the (100) planes and cut into 5×5 mm² samples. Three sets of samples were implanted

along the $\langle 201 \rangle$ surface normal with Eu (300 keV) using a fluence of 1×10^{15} at cm⁻² with a constant flux of 2.5×10^{12} at cm⁻² s. Samples of the first set were implanted in a temperature range from 20 °C to 1000 °C. A second set of samples was implanted at 300 °C and a third set at 600 °C to study the influence of the annealing temperature. Post-implant rapid thermal annealing on the second and third set of samples was performed in the temperature range from 700 °C to 1000 °C in flowing Ar during 30 s in an ANNEALSYS rapid thermal processor. The annealing temperature was limited to 1000 °C in order to avoid diffusion of Eu towards the surface [12].

To monitor the lattice disorder and the Eu lattice site location with depth resolution, RBS/C measurements were carried out using a 2 MeV He⁺ beam and a Si pin diode placed at a backscattering angle of 165°. Random and aligned spectra along the $\langle 201 \rangle$ direction were acquired to determine the minimum yield defined by the relation Y_{Al}/Y_{Rand} , where Y_{Al} and Y_{Rand} correspond to the yield of the aligned and random spectra, respectively. The defect profiles, corresponding to the relative number of displaced Ga atoms, were determined by calculating the difference between the minimum yield of the implanted and the virgin samples as a function of depth and subtracting the dechanneling yield. In order to take into account the dechanneling of beam particles at defects, the dechanneling rate was estimated using a two-beam approximation model [24, 26] following the procedure of Wendler *et al* [21].

Cathodoluminescence (CL) studies were performed at RT with a Hitachi S2500 scanning electron microscope (SEM) using an acceleration voltage of 5 keV.

The charge state of implanted Eu was measured by x-ray absorption near edge structure (XANES) collected at RT in fluorescence mode at the Eu L_{III} edge. Experiments were conducted on both the French CRG BM30B-FAME and the Spanish CRG BM25-SPLINE beamlines at the European Synchrotron Radiation Facility in Grenoble, France.

3. Results and discussion

Figure 1(a) shows the RBS/C spectra of samples implanted to the same fluence of 1×10^{15} at cm⁻² at different temperatures in the range from 20 °C to 1000 °C. The defect profiles extracted considering the range of energies between 1300 and 1600 keV, which corresponds to the region of the Ga barrier before the onset of the O-signal, are presented in figure 1(b). For comparison, the Eu and the vacancy profiles, calculated by the Monte Carlo code SRIM (version 2013 using displacement/binding energies of 25/3 eV for Ga and 28/3 eV for O) [27], are included in the figure in arbitrary units. These spectra show that, for 20 °C implantation, there are two distinct regions with one defect peak near the surface and another located deeper in the sample, between 50 and 125 nm. In more detail, it can be seen that in the sample implanted at 20 °C the aligned spectrum near the surface almost reaches the random spectra. This means that the implantation at 20 °C induces a high density of defects eventually resulting in amorphization. This high surface damage is unusual for implantation since the maximum of nuclear energy deposition is located deeper

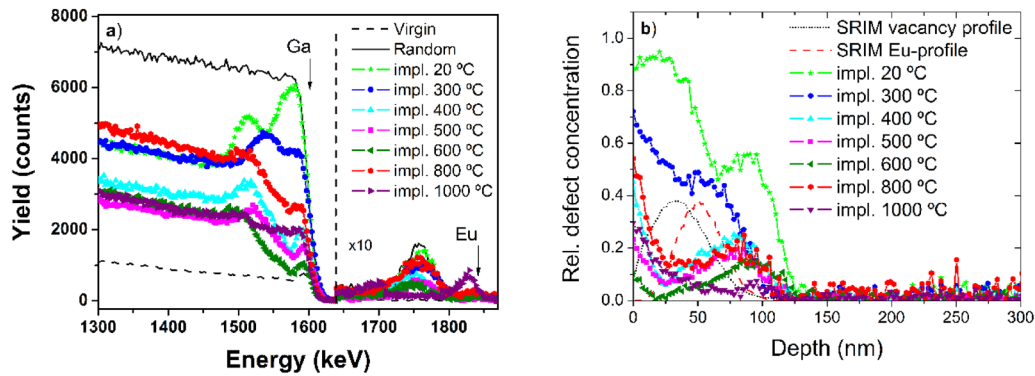


Figure 1. (a) RBS/C random and $\langle 201 \rangle$ aligned spectra for the β - Ga_2O_3 samples implanted at different temperatures. The energies corresponding to Eu and Ga signals from the surface are marked by arrows. (b) Relative defect concentration as a function of depth extracted from the RBS/C spectra in (a). For comparison, the Eu and the vacancy profiles calculated using SRIM were also inserted in arbitrary units.

inside the sample (see SRIM vacancy profile in figure 1(b)) and suggests that the surface acts as a sink for migrating defects. Similar damage profiles have been reported for an analogous RT Eu implantation in GaN [24]. It should be noted that such preferential surface damage was not observed in Ga_2O_3 with (0 1 0) surface orientation, suggesting that the surface itself with its orientation and termination is influencing the defect migration and accumulation [21]. For implantations at higher temperatures the damage near the surface is considerably reduced, achieving a minimum for implantations at 600 °C. The second peak follows a similar tendency and decreases with increasing implantation temperature up to 600 °C. Above this temperature the concentration of defects starts to increase again. A similar tendency induced by the annealing temperature during post-implant thermal treatment was observed for RT-implanted samples and attributed to defect rearrangement and/or clustering [12]. The second peak is clearly shifted to a deeper region comparatively to the position of the maximum of the vacancy profile and even compared to the maximum of the Eu profile, both calculated by SRIM. This behavior suggests migration of defects during the implantation and their accumulation close to the interface between implanted and pristine regions of the sample. This effect is evident in all samples implanted at different temperatures indicating that the diffusion associated to the implantation temperature may play a secondary role. It should be mentioned that the two-beam model employed here was developed for randomly displaced atoms only. However, the spectra seen in figure 1(a), in particular for implantation temperatures above 300 °C, are typical for extended defects such as stacking faults or dislocation loops which lead to relatively low direct backscattering but high dechanneling yields. To take this into account, the dechanneling yield in the two-beam model was increased by decreasing the critical angle of dechanneling until the defect density reaches zero in the deeper, unimplanted layers of the sample. Using this procedure a good agreement with SRIM defect profiles for low fluence Eu-implantation in the present samples was obtained [12], as well as for implantation at RT of several ion species in (0 1 0) Ga_2O_3 [21]. However, it may lead to ambiguous results in the defect profiles in the present case, where high densities of extended defects are present,

since defect profiles only reflect the direct backscattering yield due to atoms which are displaced from the atomic rows perpendicular to the channeling direction (due to a mixture of different defect microstructures) and not directly the density of extended defects. Nevertheless, it is clear from the RBS/C spectra that both direct backscattering and dechanneling are strongly reduced for implantation at elevated temperatures of about 500–600 °C. Eu diffusion to the surface sets in at 1000 °C, as can be confirmed by the shift to higher energies of the Eu peak (see figure 1(a)).

For the samples implanted at low temperature, Eu is mainly located in random sites. This is seen in the almost complete overlap of the Eu-signal in the random and aligned spectra (figure 1(a)). However, for the samples implanted at temperatures above 400 °C, the minimum yield of the Eu-signal, $\chi_{\min}(\text{Eu})$, (i.e. the ratio between the Eu yield in the aligned and random spectra) starts to decrease (45% at 400 °C, 44% at 500 °C), achieving a minimum of about 34% for the sample implanted at 600 °C. For this sample (implanted at 600 °C), a substitutional fraction of about 60% (f_S) of Eu incorporated on Ga-sites was estimated considering the relation

$$f_S = (1 - \chi_{\min}(\text{Eu})) / (1 - \chi_{\min}(\text{Ga})). \quad (1)$$

This means that even in this sample approximately 40% of Eu are incorporated in non-substitutional, random sites (more correctly in sites with a displacement from the ideal Ga sites perpendicular to the channeling direction). For 800 °C, $\chi_{\min}(\text{Eu})$ increases again. Finally, for implantation at 1000 °C Eu diffuses to the surface where it resides in random lattice sites similar to what happens in samples implanted at RT but annealed above 1000 °C [12]. These results show in a clear way that 500–600 °C is the temperature range that keeps a compromise between Eu diffusion and defect level and promotes the incorporation of Eu on substitutional sites.

Based on the results presented above we chose two implantation temperatures 300 °C (resulting in mainly randomly distributed Eu but avoiding the strong surface damage) and 600 °C (resulting in high f_S and a low density of defects) in order to perform further studies of the effect of post-implant thermal annealing. The aim of this study was to understand how the two distinct defect profiles present in these samples

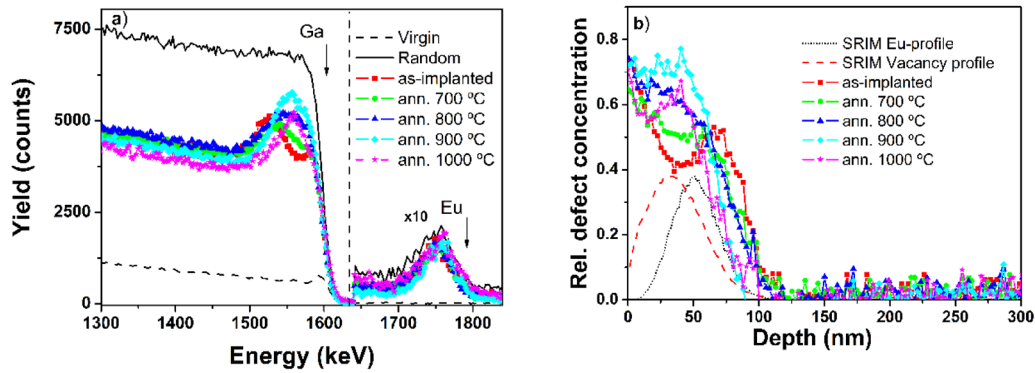


Figure 2. (a) RBS random and $\langle 201 \rangle$ aligned spectra for the as-implanted and annealed β -Ga₂O₃ samples implanted at 300 °C. The energies corresponding to Eu and Ga signals from the surface were marked by arrows. (b) Relative defect concentration as a function of depth extracted from the RBS/C spectra in (a). For comparison, the Eu and the vacancy profiles (in arbitrary units) calculated using SRIM were also inserted.

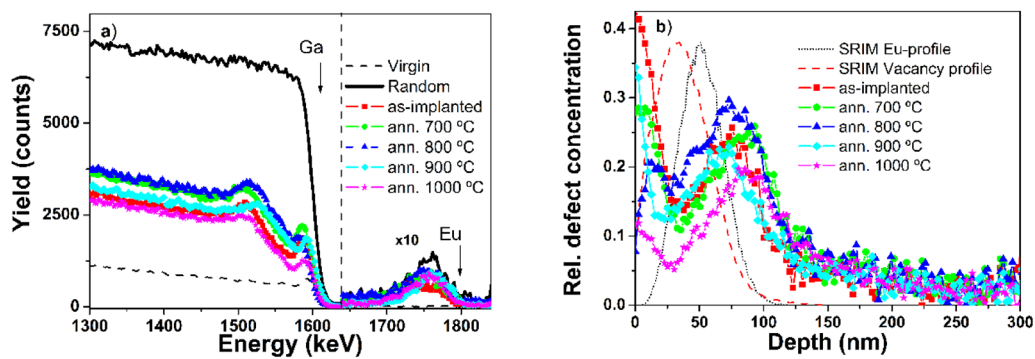


Figure 3. (a) RBS random and $\langle 201 \rangle$ aligned spectra for the as-implanted and annealed β -Ga₂O₃ samples implanted at 600 °C. The energies corresponding to Eu and Ga signals from the surface were marked by arrows. (b) Relative defect concentration as a function of depth extracted from the RBS/C spectra in (a). For comparison, the Eu profile and the vacancy profile (in arbitrary units) calculated using SRIM were also inserted.

are affected by thermal annealing and how these changes affect the f_s , the Eu charge state and ultimately the optical properties of the samples. Considering the results published in [12], in order to avoid the Eu diffusion towards the surface, the maximum annealing temperature was limited to 1000 °C

No significant changes are seen in the RBS spectra in figure 2(a) for samples implanted at 300 °C after annealing at temperatures up to 1000 °C. Although the shape of the defect profile changes slightly after each annealing step, the maximum defect level does not improve after annealing (figure 2(b)). It even increases for annealing temperatures above 700 °C similar to our results after RT implantation [12]. Only the extension of the defective region is slightly reduced with a good recovery of the crystal in a depth of 80–100 nm possibly due to regrowth starting at the interface between defective and pristine material. It is interesting to note that this regrowth does not proceed into shallower regions containing Eu (see comparison with Eu-profile calculated by SRIM in figure 2(b)). This, together with the fact that efficient defect recovery sets in at 1100 °C, when Eu diffusion becomes prominent [12], suggests that Eu and implantation defects interact and stabilize each other. Furthermore, a complete overlap of the random spectra with the aligned spectra in the region of the Eu signal is seen in all samples (figure 2(a)), indicating the incorporation of Eu in random lattice sites. This result implies

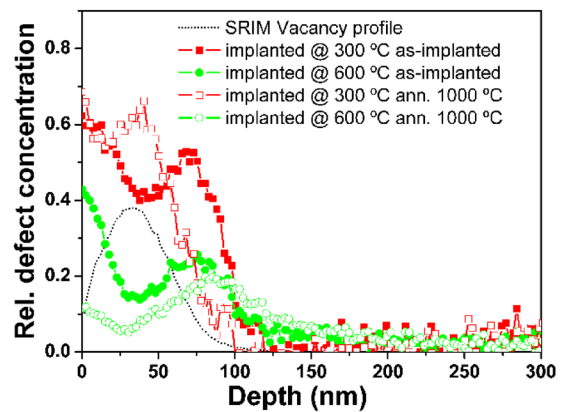


Figure 4. Relative defect concentration as a function of depth for the samples implanted at 300 °C and 600 °C before and after annealing at 1000 °C. For comparison, the vacancy profile calculated using SRIM (in arbitrary units) was also inserted.

that the annealing does not improve the f_s of Eu, being in agreement with what was already observed for similar samples implanted at RT [12].

As mentioned before, in the samples implanted at 600 °C a large percentage of Eu is incorporated on substitutional sites leading to a reduction of the Eu signal in the aligned spectrum as compared to the random spectrum. Figure 3 shows

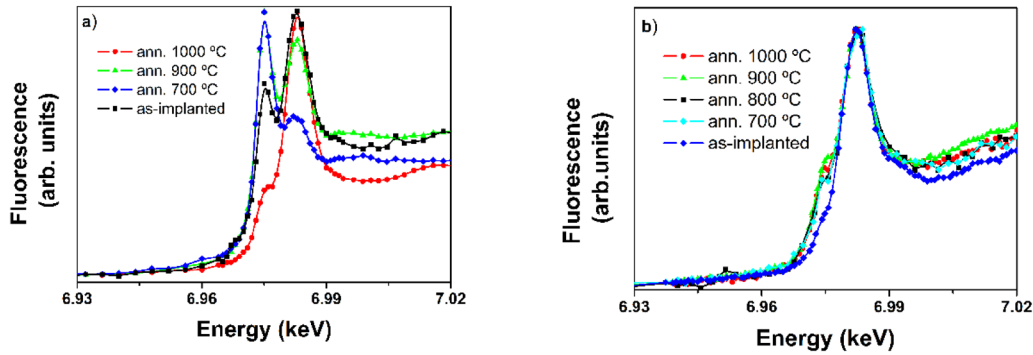


Figure 5. (a) Normalized Eu L_{III} -edge fluorescence XANES spectra of samples implanted at 300 °C (a) and 600 °C (b) after annealing at different temperatures.

that the RBS/C spectra and defect profiles in the as-implanted state and after annealing at 700 °C are almost equal, except in the near surface region where a small damage recovery is observed. A slight increase of the Eu minimum yield is noted for intermediate annealing temperatures (800 °C), accompanied by an increase of the maximum defect level for these temperatures. This increase of the relative defect concentration observed in the sample annealed at 800 °C (see figure 3(b)) is probably associated with clustering or rearrangement of defects, as mentioned above, and the simultaneous increase of $\chi_{\min}(\text{Eu})$ supports the assumption that the interaction of Eu with implantation defects prevents the incorporation of Eu on substitutional sites. For the highest annealing temperature the overall defect level is slightly reduced compared with the as-implanted sample, but the shape of the profile remains unchanged, i.e. no significant recrystallization is obtained at the interface between implanted and unimplanted material, in contrast to the samples implanted at 300 °C. These distinct tendencies for samples implanted at different temperatures support the idea that there is a strong interaction between defects (clustering), which can result in different types of extended defects with different thermal stability.

Figure 4, directly compares the effect of implantation temperature for the samples annealed at 1000 °C. The significant difference in the defect profiles is obvious. For the sample implanted at 300 °C the defect profile after annealing seems to be related with the vacancy profile calculated with SRIM. Probably the defect recombination during the implantation is low at 300 °C and the created point defects can interact to form thermally very stable defect clusters which require annealing at temperatures above 1000 °C to be removed. For implantation at 600 °C the concentration of defects is significantly reduced, suggesting a more efficient dynamic annealing, i.e. the produced point defects are mobile and recombine during the implantation, resulting in a lower relative defect concentration, which could reduce the formation of stable defect clusters. Besides a clear damage reduction for the sample implanted at 600 °C, the figure evidences a shift of the bulk defect peak maximum to a deeper position. This shift compared with the shift to the surface of the of the bulk defect peak observed in the sample implanted at 300 °C,

confirms that the elevated implantation temperature promotes a different type of defect accumulation or diffusion with thermally stable defect complexes forming preferentially at the interface between the implanted and unimplanted regions of the sample.

To understand how the different defect profiles and the f_3 affect the charge state of Eu in $\beta\text{-Ga}_2\text{O}_3$, the samples implanted at 300 °C and 600 °C were studied by XANES. The XANES technique allows identifying the charge state of Eu, due to the 8 eV difference in energy between the $2p_{3/2} \rightarrow 5d$ electronic transition for trivalent Eu^{3+} (6.982 keV) and bivalent Eu^{2+} (6.974 keV) [28, 29]. Figures 5(a) and (b) show the normalized spectra for implantation at 300 and 600 °C, respectively, after annealing at different temperatures. All spectra are characterized by the presence of the two peaks attributed to the two different charge states of Eu. These results are a clear proof of the coexistence of different charge states of Eu in $\beta\text{-Ga}_2\text{O}_3$ as already observed in Eu-doped Ga_2O_3 nanocrystals [30]. To quantify the percentage of each charge state, the normalized spectra were fitted using the following formula:

$$Y = A * P_1 * \exp[-(x - P_2)^2/P_3^2] + (1 - A) * P_1 * \exp[-(x - P_4)^2/P_3^2] + A * (1 + \text{erf}(2 * [x - P_5/P_6])) + (1 - A) * (1 + \text{erf}(2 * [x - P_7/P_6]))$$

The fractions of Eu^{3+} and Eu^{2+} are given by A and $1 - A$, respectively. $P_1 - P_4$ are fitting parameters corresponding to the intensity, energy position, and width of the two Gaussians representing the two white lines while $P_5 - P_7$ describe two error functions (erf) representing the step-like normalized absorption jump.

Figure 6 shows the tendencies of the percentage of Eu^{3+} as a function of the annealing temperature. In the samples implanted at 300 °C (figure 6(a)) the amount of Eu^{3+} first decreases strongly for annealing at 700 °C and then increases with the annealing temperature. The strong decrease of the fraction of Eu^{3+} for intermediate annealing temperatures coincides with the increase of the defect level in the region of highest Eu-content (figure 2(b)). This suggests that defects interact with Eu which tends to favor the 2+ charge state. For the highest annealing temperature of 1000 °C, the percentage of Eu^{3+} reaches a maximum of close to 80% which is in fair agreement with the slight decrease of defect level in this

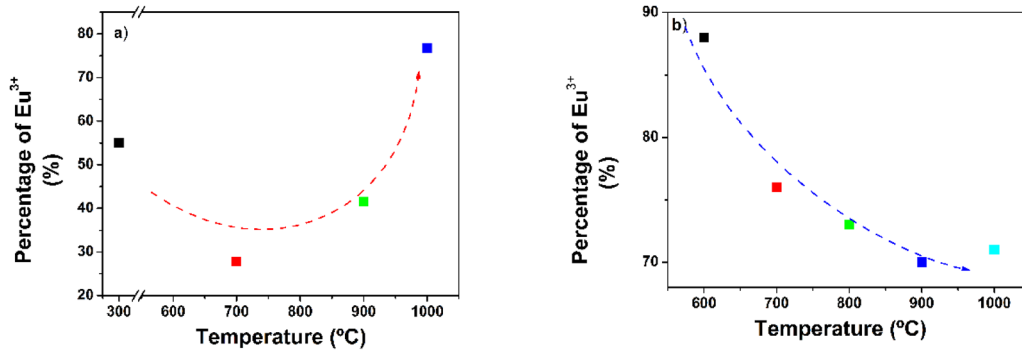


Figure 6. Percentage of Eu^{3+} as a function of the annealing temperature for the samples implanted at 300 °C (a) and at 600 °C (b). (The dashed lines are guides for the eyes).

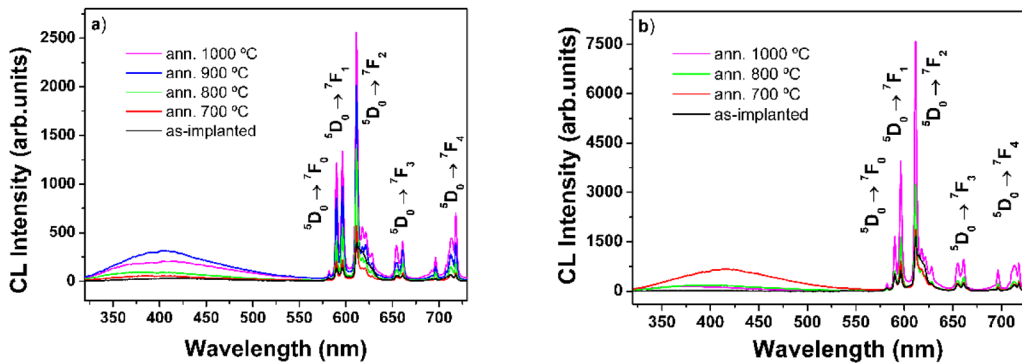


Figure 7. RT CL spectra of $\beta\text{-Ga}_2\text{O}_3$ samples implanted at 300 °C (a) and at 600 °C (b) annealed at different temperatures.

sample. However, as shown by the RBS/C measurements this is not an effect of substitutional incorporation of Eu in Ga-sites. In fact, the random lattice sites of Eu rather point to the incorporation of Eu in a distinct defect configuration that promotes the Eu^{3+} state.

Directly after implantation at 600 °C (figure 6(b)), the percentage of Eu^{3+} reaches nearly 90% significantly higher than for implantation at 300 °C (55%). This evidence is in good agreement with the lower defect level present in the sample implanted at 600 °C. However, this percentage then diminishes with increasing annealing temperature, similar to the samples implanted at 300 °C and again in agreement with increasing defect levels at intermediate temperatures. Figure 6(b) illustrates this decrease of the Eu^{3+} fraction with the annealing temperature, reaching a minimum value slightly above 70% for annealing at 900 °C. After 1000 °C annealing, the Eu^{3+} fraction is comparable with the value achieved for the same annealing conditions in the samples implanted at 300 °C. Considering the similar Eu^{3+} percentage observed in these two samples implanted at 300 °C (with Eu mostly in random lattice sites) and 600 °C (with Eu mostly in substitutional lattice sites), no obvious relation can be established between the charge state and the substitutional fraction. The strong dependence of Eu^{3+} percentage on implantation and annealing temperature confirms that the concentration and type of defects play an important role, affecting the coordination environment of Eu. Our results indicate that an increase of the RBS/C backscattering yield (presumably due the formation of defect clusters) is correlated with an increase of the Eu^{2+} fraction. However, the exact mechanisms and defects at

the atomic scale need to be studied further, for example by transmission electron microscopy, in order to gain insight into the interaction of defects with Eu. In any case, it is noteworthy that the Eu ratios tend to converge to the same value after annealing at high temperatures, independently of the implantation temperature and in spite of the remarkable difference in concentration and location of defects (see figure 4).

Figures 7(a) and (b) show the CL spectra for the samples implanted at 300 °C and 600 °C, respectively. All spectra present a broad band around 400 nm, which has been attributed to transitions involving donors and acceptors associated to intrinsic point defects, such as oxygen vacancies, gallium vacancies and oxygen-gallium vacancy pairs [31–34]. Our results indicate that its shape and intensity depend on the annealing and implantation conditions. However, no direct correlation with the annealing temperature, nor with the implantation temperature was found. The absence of a clear trend could be explained by the fact that different processes involving different defects could be associated to this band. Considering the XANES results, the influence of Eu^{2+} on the presence of this broad band in the implanted samples cannot be excluded [35], but is difficult to confirm due to the overlap of several bands. To further discuss the nature of this band it is necessary to perform complementary studies as for example studies at different temperatures or excitation densities.

In addition to these bands, localized at lower wavelengths, the CL spectra are dominated by the sharp and intense luminescence lines assigned to the $^5\text{D}_0 \rightarrow ^7\text{F}_j$ intra-ionic transitions of Eu^{3+} . These results are in agreement with the XANES measurements, which showed that a large fraction of the ions are

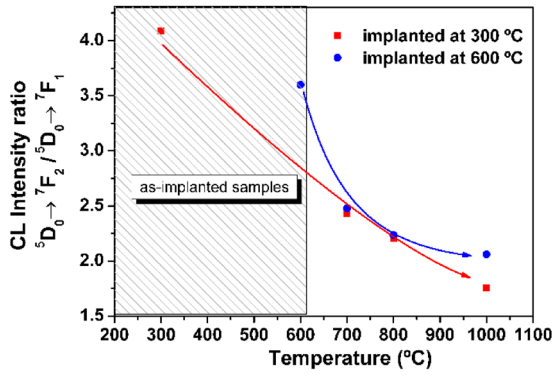


Figure 8. CL intensity ratio of the ${}^5D_0 \rightarrow {}^7F_2$ to the ${}^5D_0 \rightarrow {}^7F_1$ transition (the solid lines are a guide for the eyes).

found in the 3+ valence state. In both sample sets, implanted at 300 °C and at 600 °C, the most intense line is the hypersensitive ${}^5D_0 \rightarrow {}^7F_2$ transition, which points to Eu^{3+} ions in a low site symmetry without an inversion center [36]. Considering that pure magnetic-dipole transitions (as the ${}^5D_0 \rightarrow {}^7F_1$ transition) are practically insensitive to the local environment in contrast to the hypersensitive ${}^5D_0 \rightarrow {}^7F_2$ electric-dipole transition, the intensity ratio between these two transitions is a good way to evaluate the local symmetry of the optically active Eu centers [36]. In our case, the decrease of this ratio with increasing annealing temperature (figure 8) suggests the presence of multiple optically active centers and indicates that the annealing treatment promotes the optical activation of the Eu centers with higher symmetry. In $\beta\text{-Ga}_2\text{O}_3$, and not taking into account possible effects of defects, the most likely sites with low symmetry that keep the charge neutrality with respect to the matrix are the two Ga-sites with octahedral and tetrahedral coordination. As pointed out by Zhu *et al*, these two sites have a Cs symmetry because in $\beta\text{-Ga}_2\text{O}_3$ the tetrahedron and the octahedron are not regular but distorted [15]. However, the octahedral site is more probable because the ionic radius of Ga in this site is considerably larger than that in the tetrahedral site (0.062 and 0.047 nm, respectively), thus allowing an easier accommodation of the Eu^{3+} ion with an ionic radius of 0.095 nm [15]. Indeed, Zhu *et al* [15] reported that emitting Eu^{3+} in $\beta\text{-Ga}_2\text{O}_3$ nanocrystals is only found in the octahedral site.

Taking into account the work of Zhu *et al* [15] and considering that most of the Eu ions in the samples implanted at 300 °C are found in random sites (as shown by RBS/C), we can conclude that either the luminescence is caused by only a small percentage of the ions which indeed are incorporated in substitutional sites or that other optical centers, most probably involving defects, exist in our samples. In fact, the shape and energy positions of the observed Eu intraionic transitions do not exactly match those reported for substitutional Eu in Ga_2O_3 [15]. The optical spectra differ in the number of peaks attributed to the ${}^5D_0 \rightarrow {}^7F_1$ transition (two peaks in our work instead of three) and in the emission wavelength of the ${}^5D_0 \rightarrow {}^7F_4$ transition (with the most intense line found at ~ 705 nm in [15] and at 717 nm in our work). While the lower number of peaks can be due to a lower spectral resolution of our acquisition system or a stronger peak broadening due to

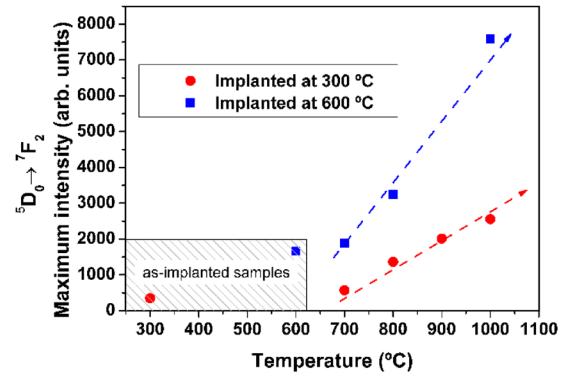


Figure 9. Maximum intensity of the ${}^5D_0 \rightarrow {}^7F_2$ transition as a function of the annealing temperature for the samples implanted at 300 °C and 600 °C (the dashed lines are guides for the eyes).

implantation defects, the difference in the energy position of the ${}^5D_0 \rightarrow {}^7F_4$ transition suggests a different crystal field splitting of the 7F_4 level. This can only be justified considering that Eu is in a different crystalline environment caused by different (non-substitutional) sites or in substitutional sites with distortion induced by defects. An alternative explanation to these discrepancies is to consider that the observed emission is coming from Eu in nanoscopic clusters of Eu_2O_3 , as suggested by other authors [37]. Despite the similarities with the spectra reported in [37], our spectra do not match the shape and the peak positions of the typically observed Eu emissions in Eu_2O_3 [38–40].

Figure 9 shows the dependence of the CL peak intensity of the ${}^5D_0 \rightarrow {}^7F_2$ transition as a function of the annealing temperature for the samples implanted at 300 and 600 °C. The intensity for the as-implanted sample at 600 °C is almost three times higher than that of the as-implanted sample at 300 °C. This difference can either be related to the substitutional fraction, found to be considerably higher in the samples implanted at 600 °C, or to the defect concentration, which is significantly higher for the samples implanted at 300 °C and can favor non-radiative recombination. Furthermore, for both sample sets, a strong increase of the luminescence intensity with the annealing temperature is seen. Despite the similar trend, this increase is significantly steeper for the samples implanted at 600 °C. In fact, the intensity increases by a factor of 10 between the as-implanted sample and that annealed at 1000 °C, in comparison to a 6 fold increase observed on the samples implanted at 300 °C. Considering the XANES results which showed a strong decrease of the Eu^{3+} percentage with increasing annealing temperature in the sample implanted at 600 °C, we can assume that the local symmetry of the optical centers and the excitation and recombination processes play the main role determining the emission intensity, rather than the Eu^{3+} concentration itself. Thermal annealing is expected to reduce the inhomogeneous strain induced by defects and can therefore affect the local site symmetry of the RE ions. In our case this effect is corroborated by the sharpening of the emission peaks with increasing annealing temperature (see figures 7(a) and (b)) in agreement with results on ion implanted Ga_2O_3 nanowires [41].

4. Conclusion

In conclusion, implantation at intermediate temperatures around 600 °C successfully reduced implantation damage in Eu-implanted Ga₂O₃, while promoting the incorporation of Eu into substitutional sites in the 3+ charge state, and improving the optical activation of Eu ions. Accumulation of implantation damage was found to be a complex process. The damage level of as-implanted samples was shown to decrease significantly when raising the implantation temperature to 400–600 °C which is attributed to efficient dynamic annealing. Increasing further the implantation temperature enhances the damage retained after implantation again, pointing to a clustering of defects to form thermally stable complexes. Similar effects are seen for post-implant annealing where indeed damage levels first increase for intermediate annealing temperatures and only start to decrease for the highest temperatures of ~900–1000 °C. In fact, Eu and defects seem to stabilize each other since efficient damage recovery is accompanied by out-diffusion of Eu. This is seen for post-implant annealing above 1000 °C [12] as well as for implantation at 1000 °C.

XANES measurements reveal the coexistence of Eu in 2+ and 3+ charge states with ratios that depend strongly on the implantation and annealing temperature. As-implanted samples implanted at 600 °C have a high fraction of Eu³⁺, almost 90%, which is in good agreement with an increased substitutional fraction measured by RBS/C. As-implanted samples implanted at 300 °C, on the other hand, show a much lower Eu³⁺ fraction of around 55%.

Annealing promotes an efficient optical activation of the Eu³⁺ ions since the CL intensity of their typical transition lines increases strongly with the annealing temperature. However, no direct correlation is found between emission intensity, substitutional fraction and Eu³⁺/Eu²⁺ ratio, suggesting that defects play a major role in the observed optical and charge state properties.

Acknowledgments

M Peres thanks FCT, Portugal for his post-doc grant, SFRH/BPD/111285/2015 and K Lorenz for the grant as Investigador FCT. Support by the bilateral PESSOA project FCT/EGIDE is gratefully acknowledged. B Méndez and E Nogales thank financial support from Spanish Minister through project MAT 2012-31959, MAT 2015-65274-R/FEDER and Consolider CSD 2009-00013.

ORCID

M Peres  <https://orcid.org/0000-0001-6774-8492>

B Méndez  <https://orcid.org/0000-0002-6289-7437>

References

- [1] Vllora E G, Arjoca S, Shimamura K, Inomata D and Aoki K 2014 β -Ga₂O₃ and single-crystal phosphors for high-brightness white LEDs and LDs, and β -Ga₂O₃ potential for next generation of power devices *Proc. SPIE* **8987** 89871U
- [2] Tippins H 1965 Optical absorption and photoconductivity in the band edge of β -Ga₂O₃ *Phys. Rev.* **140** A316–9
- [3] Mohamed M, Janowitz C, Unger I, Manzke R, Galazka Z, Uecker R, Fornari R, Weber J R, Varley J B and Van De Walle C G 2010 The electronic structure of β -Ga₂O₃ *Appl. Phys. Lett.* **97** 2008–11
- [4] Schubert M *et al* 2016 Anisotropy, phonon modes, and free charge carrier parameters in monoclinic β -gallium oxide single crystals *Phys. Rev. B* **93** 125209
- [5] Hwang W S *et al* 2014 High-voltage field effect transistors with wide-bandgap β -Ga₂O₃ nanomembranes *Appl. Phys. Lett.* **104** 3–8
- [6] Wellenius P, Smith E R, Leboeuf S M, Everitt H O and Muth J F 2010 Optimal composition of europium gallium oxide thin films for device applications *J. Appl. Phys.* **107** 2–7
- [7] Chen Z, Wang X, Zhang F, Noda S, Saito K, Tanaka T, Nishio M, Arita M and Guo Q 2016 Observation of low voltage driven green emission from erbium doped Ga₂O₃ light-emitting devices *Appl. Phys. Lett.* **22107** 15–9
- [8] Muhammed M M, Peres M, Yamashita Y, Morishima Y, Sato S, Franco N, Lorenz K, Kuramata A and Roqan I S 2014 High optical and structural quality of GaN epilayers grown on (201) β -Ga₂O₃ *Appl. Phys. Lett.* **105** 42112
- [9] Villora E G, Shimamura K, Kitamura K, Aoki K and Ujjie T 2007 Epitaxial relationship between wurtzite GaN and β -Ga₂O₃ *Appl. Phys. Lett.* **90** 234102
- [10] Varley J B, Weber J R, Janotti A and Van de Walle C G 2010 Oxygen vacancies and donor impurities in β -Ga₂O₃ *Appl. Phys. Lett.* **97** 142106
- [11] Santos N F, Rodrigues J, Fernandes A J S, Alves L C, Alves E, Costa F M and Monteiro T 2012 Optical properties of LFZ grown β -Ga₂O₃:Eu³⁺ fibres *Appl. Surf. Sci.* **258** 9157–61
- [12] Lorenz K *et al* 2014 Doping of Ga₂O₃ bulk crystals and NWs by ion implantation *Proc. SPIE* **8987** 89870M
- [13] Nogales E, Hidalgo P, Lorenz K, Méndez B, Piqueras J and Alves E 2011 Cathodoluminescence of rare earth implanted Ga₂O₃ and GeO₂ nanostructures *Nanotechnology* **22** 285706
- [14] López I, Castaldini A, Cavallini A, Nogales E, Méndez B and Piqueras J 2014 β -Ga₂O₃ nanowires for an ultraviolet light selective frequency photodetector *J. Phys. D.: Appl. Phys.* **47** 415101
- [15] Zhu H, Li R, Luo W and Chen X 2011 Eu³⁺-doped β -Ga₂O₃ nanophosphors: annealing effect, electronic structure and optical spectroscopy *Phys. Chem. Chem. Phys.* **13** 4411–9
- [16] Kenyon A J 2002 Recent developments in rare-earth doped materials for optoelectronics *Prog. Quantum Electron.* **26** 225–84
- [17] Rodrigues J *et al* 2015 Spectroscopic analysis of Eu³⁺ implanted and annealed GaN layers and nanowires *J. Phys. Chem. C* **119** 17954–64
- [18] Lupan O, Viana B, Pauporte T, Dhaouadi M, Pelle F, Devys L and Gacoin T 2013 Controlled mixed violet–blue–red electroluminescence from Eu: nano-phosphors/ZnO-nanowires/p-GaN light-emitting diodes *J. Phys. Chem. C* **117** 26768–75
- [19] Nogales E, Garcia J A, Mendez B, Piqueras J, Lorenz K and Alves E 2008 Visible and infrared luminescence study of Er doped β -Ga₂O₃ and Er₃Ga₅O₁₂ *J. Phys. D.: Appl. Phys.* **41** 65406
- [20] Higashiwaki M, Sasaki K, Kuramata A, Masui T and Yamakoshi S 2014 Development of gallium oxide power devices *Phys. Status Solidi* **211** 21–6
- [21] Wendler E, Treiber E, Baldauf J, Wolf S and Ronning C 2016 High-level damage saturation below amorphisation in ion implanted *Nucl. Instrum. Methods Phys. Res. B* **379** 85–90

- [22] Mejai N, Debelle A, Thomé L, Sattonnay G, Gosset D, Boule A, Dargis R and Clark A 2015 Depth-dependent phase change in Gd_2O_3 epitaxial layers under ion irradiation *Appl. Phys. Lett.* **107** 131903
- [23] Lorenz K, Wahl U, Alves E, Dalmaso S, Martin R W and O'Donnell K P 2003 High temperature implantation of Tm in GaN *Materials Research Society Symp. Proc.* vol 798 pp 447–52
- [24] Lorenz K, Barradas N P, Alves E, Roqan I S, Nogales E, Martin R W, O'Donnell K P, Gloux F and Ruterana P 2009 Structural and optical characterization of Eu-implanted GaN *J. Phys. D.: Appl. Phys.* **42** 165103
- [25] Villora E G, Shimamura K, Yoshikawa Y, Aoki K and Ichinose N 2004 Large-size $\beta\text{-Ga}_2\text{O}_3$ single crystals and wafers *J. Cryst. Growth* **270** 420–6
- [26] Bøgh E 1968 Defect studies in crystals by means of channeling *Can. J. Phys.* **46** 653–62
- [27] Ziegler J F, Ziegler M D and Biersack J P 2010 SRIM—the stopping and range of ions in matter *Nucl. Instrum. Methods Phys. Res. B* **268** 1818–23
- [28] Beaurepaire E, Kappler J P and Krill G 1986 Xanes study of trivalent and homogeneous mixed valent rare earth systems *Solid State Commun.* **57** 145–9
- [29] Wortmann G 1989 Edge spectroscopy *Hyperfine Interact.* **47–8** 179–202
- [30] Layek A, Yildirim B, Ghodsi V, Hutfluss L N, Hegde M, Wang T and Radovanovic P V 2015 Dual europium luminescence centers in colloidal Ga_2O_3 nanocrystals: controlled *in situ* reduction of Eu(III) and stabilization of Eu(II) *Chem. Mater.* **27** 6030–7
- [31] Onuma T, Fujioka S, Yamaguchi T, Higashiwaki M, Sasaki K, Masui T and Honda T 2013 Correlation between blue luminescence intensity and resistivity in $\beta\text{-Ga}_2\text{O}_3$ single crystals *Appl. Phys. Lett.* **103** 3–6
- [32] Harwig T and Kellendonk F 1978 Some observations on the photoluminescence of doped $\beta\text{-galliumsesquioxide}$ *J. Solid State Chem.* **24** 255–63
- [33] Binet L and Gourier D 1998 Origin of the blue luminescence of $\beta\text{-Ga}_2\text{O}_3$ *J. Phys. Chem. Solids* **59** 1241–9
- [34] Zhang J et al 2006 Growth and spectral characterization of $\beta\text{-Ga}_2\text{O}_3$ single crystals *J. Phys. Chem. Solids* **67** 2448–51
- [35] Chen P, Zhou L, Mo F, Guan A, Huang N, Gan Y, Chen M and Zhang W 2015 A novel blue luminescent material $\text{Sr}_6\text{Ca}_4(\text{PO}_4)_6\text{F}_2\text{:Eu}^{2+}$ *Mater. Res. Bull.* **72** 191–6
- [36] Binnemans K 2015 Interpretation of europium (III) spectra *Coord. Chem. Rev.* **295** 1–45
- [37] Chen Z, Saito K, Tanaka T, Nishio M, Arita M and Guo Q 2015 Low temperature growth of europium doped Ga_2O_3 luminescent films *J. Cryst. Growth* **430** 28–33
- [38] Bihari B, Eilers H and Tissue B M 1997 Spectra and dynamics of monoclinic Eu_2O_3 and $\text{Eu}^{3+}\text{:Y}_2\text{O}_3$ nanocrystals *J. Lumin.* **75** 1–10
- [39] Bazzi R et al 2004 Synthesis and properties of europium-based phosphors on the nanometer scale: Eu_2O_3 , $\text{Gd}_2\text{O}_3\text{:Eu}$, and $\text{Y}_2\text{O}_3\text{:Eu}$ *J. Colloid Interface Sci.* **273** 191–7
- [40] Sheng K C and Korenowski G M 1988 Laser-induced optical emission studies of Eu^{3+} sites in polycrystalline powders of monoclinic and body-centered cubic Eu_2O_3 *J. Phys. Chem.* **4** 50–6
- [41] López I, Lorenz K, Nogales E, Méndez B, Piqueras J, Alves E and García J A 2014 Study of the relationship between crystal structure and luminescence in rare-earth-implanted Ga_2O_3 nanowires during annealing treatments *J. Mater. Sci.* **49** 1279–85